Amino Acidic Control of Calcium Phosphate Precipitation by Using the Vapor Diffusion Method in Microdroplets

ARTICLE *in* CRYSTAL GROWTH & DESIGN · NOVEMBER 2011

Impact Factor: 4.89 · DOI: 10.1021/cg2004547

5 AUTHORS, INCLUDING:

Jaime Gómez-Morales
Spanish National Research Council
77 PUBLICATIONS **1,291** CITATIONS
SEE PROFILE

Jose Manuel Delgado López
To.Sca.Lab (University of Insubria & CNR, Co…
43 PUBLICATIONS **485** CITATIONS
SEE PROFILE

Michele Iafisco
Italian National Research Council
72 PUBLICATIONS **994** CITATIONS
SEE PROFILE

Maria Prat
Amedeo Avogadro University of Eastern Pied…
141 PUBLICATIONS **4,315** CITATIONS
SEE PROFILE

CRYSTAL GROWTH & DESIGN

ARTICLE

pubs.acs.org/crystal

Amino Acidic Control of Calcium Phosphate Precipitation by Using the Vapor Diffusion Method in Microdroplets

Jaime Gómez-Morales,*[,†] José Manuel Delgado-López,[†] Michele Iafisco,[‡,§] Angeles Hernández-Hernández,[†] and María Prat[§]

[†]Laboratorio de Estudios Cristalográficos, IACT (CSIC-UGR), 1.5 Av. Las Palmeras 4, E-18100 Armilla, Spain

[‡]Dipartimento di Chimica "G. Ciamician", Alma Mater Studiorum, Università di Bologna, Via Selmi 2, 40126 Bologna, Italy

[§]Dipartimento di Scienze Mediche, Università de Piemonte Orientale, Via Solaroli 4, 28100 Novara, Italy

ABSTRACT:

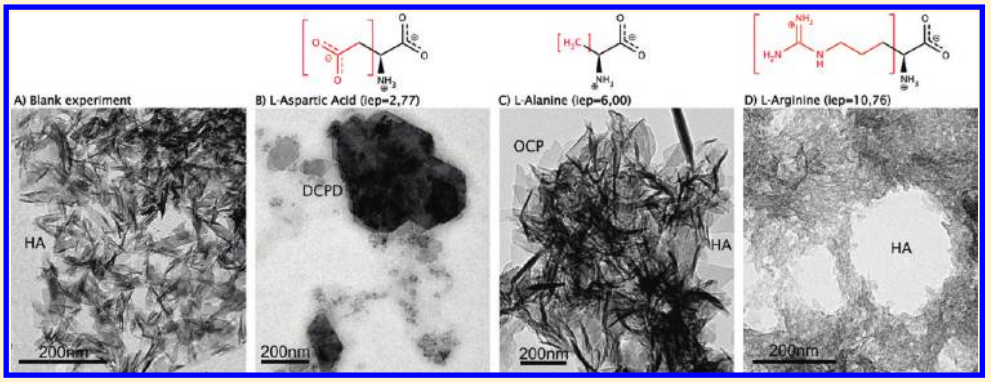

Calcium phosphate precipitation was carried out in the presence of L-aspartic acid (L-asp, iep = 2.77), L-alanine (L-ala, iep = 6.00), and L-arginine (L-arg, iep = 10.76) at different concentrations by using a vapor diffusion sitting drop method (VDSD) in microdroplets. Irrespective of the nature and the concentration of the amino acid used, the early stage in the precipitation consisted in the formation of a white viscous suspension composed of amorphous calcium phosphate (ACP) spherulites. After 1 week, different calcium phosphate phases were found depending on the amino acid nature and concentration. At higher concentrations of L-aspartic acid, brushite (dicalcium phosphate dihydrate, DCDP) platelets and a few needle-like carbonate-hydroxyapatite (HA) crystals were found. In the presence of higher concentrations of L-alanine, the precipitate was composed of both needle-like HA and octacalcium phosphate (OCP) platelets. Finally, at higher concentrations of L-arginine, we obtained carbonate-HA nanocrystals with length of 20−40 nm and a few OCP crystals, as in the blank experiment (without amino acids). The results are explained on the basis of the influence of these amino acids on the pH evolution of the solution and on the nature and strength of the interactions of the major charged species of the amino acids with the surface lattice ions of the apatite precursor phases (DCPD or OCP). A thermodynamic model, based on the temporal existence of OCP in the solution, is proposed to explain the formation of the HA nanocrystals.

INTRODUCTION

The crystallization mechanisms of bioinorganic crystals in the presence of organic additives are of fundamental importance in biomineralization as well as in the biomaterial field.[1] The organic−inorganic interface is essential, since it provides the active sites for biological control, by which the nature organizes the nucleation, growth, and morphology of the inorganic crystals and the function of biomolecules.[2,3] Thus, inspired by the nature, the molecular manipulation of inorganic crystals with organic molecules gradually has been developing into a powerful tool for the design of novel biomaterials. In fact, the synthesis of inorganic crystals in the presence of different biomolecules in terms of size and charge allows tailoring of their morphology, size, and crystallinity degree.[4,5]

Hydroxyapatite ($Ca_5(PO_4)_3OH$), the thermodynamically most stable calcium phosphate (CaP) phase under physiological conditions, represents the model compound of the inorganic constituent of bone, teeth, and many pathological calcifications.[6] Bone apatites are poorly crystalline calcium deficient crystals (Ca/P < 1.67) with sizes within the following dimensions: length of 30−50 nm, width of 30−50 nm, and thickness of 2−10 nm.[1,6] In addition, they usually present several foreign ions into the crystalline structure such as carbonate (4−6%), Na (0.9%), Mg (0.5%), and others.[1,5] Hereafter we will use the abbreviation HA to refer to apatites.

HA is preferentially formed under neutral or basic conditions. In more acidic solutions, other CaP phases such as dicalcium phosphate dihydrate (brushite, $CaHPO_4 \cdot 2H_2O$, DCPD) and

Received: April 11, 2011
Revised: September 23, 2011
Published: September 28, 2011

octacalcium phosphate ($Ca_8H_2(PO_4)_6 \cdot 5H_2O$; OCP) are often found. However, in normal *in vivo* calcifications these phases have not been found, suggesting the involvement of other precursors or the formation of an initial amorphous calcium phosphate phase ($Ca_9(PO_4)_6 \cdot xH_2O$; ACP) followed by transformation to HA.[7]

Synthetic nanocrystalline HA with physicochemical features close to those of bone HA is of great interest in the preparation of HA-based materials for biomedical applications in bone substitution, repair, or augmentation, or as potential carrier vehicles for drugs, proteins, and genes delivery.[5,6] For these applications the presence of amino acids during the synthesis has recently been postulated as a methodology to enhance their bioactivity and their selective loading capacity for proteins.[8] Nevertheless, the production of nanoparticles in the presence of amino acids is a very complex process, since they can interfere with the mechanisms of CaP precipitation at the molecular level. In fact, acidic amino acids can inhibit the crystal growth of HA when they are present in a solution[9,10] or promote crystal nucleation when they are absorbed onto a matrix.[10] Amino acids can influence the initial precipitated metastable solid phase and its further transformation to the more stable HA phase[11] as well as its crystallinity, size, and morphology.[12,13] Therefore, the role of acidic and basic amino acids on the crystallization mechanisms of CaP by using a given crystallization technique deserves detailed study because they could have a potential role as polymorph directing agents favoring the formation of a given CaP phase with given physicochemical and morphological features.

Despite the large number of different synthetic strategies to prepare nanosized HA crystals,[14] the preparation of biomimetic nanoapatites, with characteristics similar to those of bone HA, still remains an intellectual and technological challenge. Recently, we reported for the first time a new methodology to precipitate biomimetic HA nanoparticles[15] and other calcium phosphates[16] by the vapor diffusion sitting drop (VDSD) micromethod. This micromethod was also employed several times for *in vitro* studies of $CaCO_3$ both in the absence and in the presence of proteins[17,18] and biological fluids.[19] Vapor diffusion in milliliter scale vessels has been employed also by other authors to obtain biomimetic HA.[20,21] The two main features of the VDSD method are the control of the gas diffusion rate (NH_3 and CO_2) by simply changing the concentration of NH_4HCO_3 and the confinement of the nucleation in microdroplets that closely resemble the *in vivo* microenvironments where biominerals are deposited. By doing so, it is possible to control the rate of pH increase until it reaches an asymptotic value and therefore the rate of droplets supersaturation. A low rate of pH increase improves the crystal quality, while a variation in the rate of pH increase allows screening of the kinetics of crystal formation. Another advantage of the method described here is the possibility to perform several experiments per run, since as many as 12 drops per mushroom can be used.

In the present work we have investigated the effects of acidic and basic amino acids on the precipitation of CaP by this technique. For this study we used amino acids with different isoelectric points, such as L-aspartic acid (L-asp, iep = 2.77), L-alanine (L-ala, iep = 6.00), and L-arginine (L-arg, iep = 10,76),[22] at different concentrations. The aim was twofold: (i) to produce biomimetic nanoapatites and (ii) to evaluate the amino acidic potential role as polymorph directing agents in CaP precipitation in a pH-drift vapor diffusion environment.

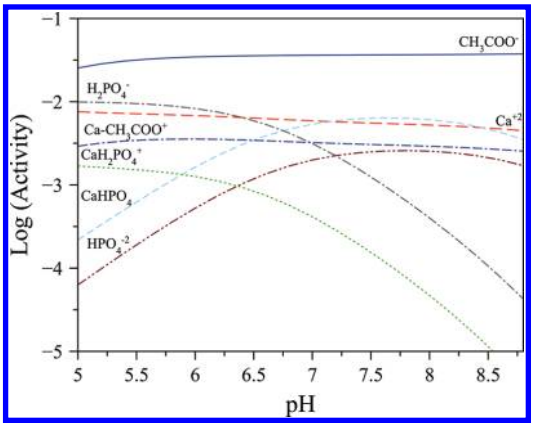

Figure 1. Activity evolution versus pH of the main calcium, acetate, and phosphate species and ion pairs in the mother solution at 25 °C. Calculated with Visual MINTEQA2 speciation software.[23]

EXPERIMENTAL SECTION

Materials. Common high-purity chemical reagents, L-arginine (98%), L-alanine (99%), and L-aspartic acid (98%), were supplied by Sigma. Ultrapure water (0.22 mS, 25 °C) was used in all experiments.

Crystallization Method. The VDSD method used in this work consists of the diffusion of NH_3 and CO_2 vapors resulting from the decomposition of an aqueous NH_4HCO_3 solution through aqueous droplets containing $Ca(CH_3COO)_2$, $(NH_4)_2HPO_4$, and one of the following amino acids, L-asp, L-ala, and L-arg. The diffusion of $NH_{3(g)}$ increases the pH of the droplets until it reaches an asymptotic value, thus producing the destabilization of the $Ca(CH_3COO)^+$ complexes and further precipitation of CaP while the diffusion of CO_2 favors the substitution of carbonate into the apatitic crystal lattice.[15] Figure 1 shows the activity evolution versus pH of the main calcium, acetate, and phosphate species and ion pairs in the mother solution in the pH range between 5.0 and 9.0. They were calculated by using the speciation program Visual MINTEQA2.[23] For the sake of simplicity, the activities of the carbonate species, ammonium, as well as of the amino acids have not been considered in the calculations. Figure 1 shows that the activity of the ionic $CaH_2PO_4^+$ pair is higher at lower pH and it decreases when increasing the pH whereas the activity of the neutral $CaHPO_4^0$ pair increases with the pH. It should be noted that previous studies on HA precipitation have identified these calcium phosphate pairs as the CaP growth units.[24]

Equations 1−3 illustrate the whole precipitation process (Ca-deficient carbonate-HA is taken as the precipitated phase):

(a) Gas generation

$$NH_{4(aq)}^+ + OH^- \leftrightarrow NH_{3(aq)} + H_2O \leftrightarrow NH_{3(g)} \quad (1)$$

$$HCO_3^-(aq) + H^+ \leftrightarrow CO_{2(aq)} + H_2O \leftrightarrow CO_{2(g)} \quad (2)$$

(b) Precipitation in droplets

$$\begin{aligned}(5-x)Ca(CH_3COO)_2 &+ (3-x)(NH_4)_2HPO_4 \\ &+ (1-x)NH_4OH + xCO_2 \\ &+ xH_2O \leftrightarrow Ca_{5-x}(PO_4)_{3-x}(CO_3)_x(OH)_{1-x} \\ &+ 2(5-x)CH_3COO^- + (7-3x)NH_4^+ \\ &+ (3+x)H^+ \quad \text{with} \quad 0 \le x \le 1\end{aligned} \quad (3)$$

The crystallization experiments were carried out in a *crystallization mushroom* (Triana Sc. & Tech, S.L.) at 20 °C and 1 atm total pressure

dx.doi.org/10.1021/cg2004547 |*Cryst. Growth Des.* 2011, 11, 4802–4809

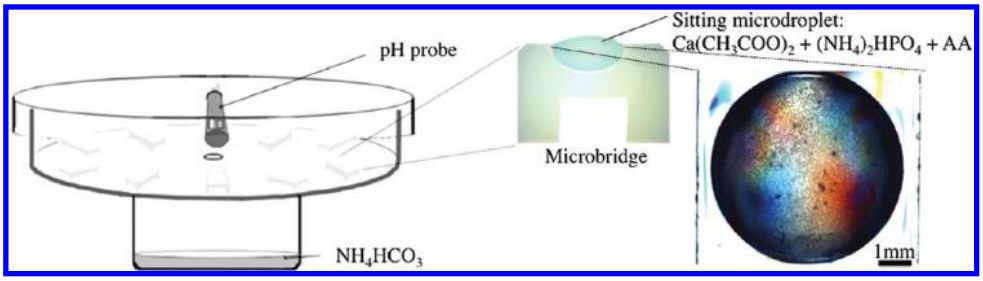

Figure 2. Experimental setup showing the *crystallization mushroom* and a large view of a microdroplet of the blank experiment containing HA nanoparticles and OCP crystals.

(Figure 2). The setup is composed of two cylindrical glass chambers and a glass cover. The crystallization chamber (upper) and the gas generation chamber (lower) are connected through a hole of 6 mm diameter to allow vapor diffusion. The glass cover and the crystallization chamber are sealed with silicon grease. In this *mushroom*, 12 polystyrene microbridges (small plastic blocks with a shallow well holding 40 μL solutions, Hampton Research, Inc.) are concentrically placed inside the crystallization chamber.

First, a set of preliminary experiments were carried out by varying the initial concentrations of $Ca(CH_3COO)_2$ and $(NH_4)_2HPO_4$ in the droplets but keeping constant the ratio Ca/P = $^5/_3$, while using 3 mL of a 40 mM $(NH_4)_2HPO_4$ solution to generate CO_2 and NH_3 gases. From these experiments we selected 25 mM $Ca(CH_3COO)_2$ and 15 mM $(NH_4)_2HPO_4$ as the reference concentrations for the blank experiment and for further crystallization experiments in the presence of amino acids. Therefore, each microbridge contained 40 μL of a solution composed of 25 mM $Ca(CH_3COO)_2$ + 15 mM $(NH_4)_2HPO_4$ as well as 5, 30, or 60 mM of each amino acid. The microbridges were filled with 20 μL of a solution of $Ca(CH_3COO)_2$ plus amino acid and then 20 μL of the $(NH_4)_2HPO_4$ solution. Finally, a crystallization experiment was performed under the same conditions as the blank but using HEPES buffer solution (pH around 8.5) and 60 mM L-Asp. The chamber for gas generation contained 3 mL of a 40 mM NH_4HCO_3 solution in all experiments. After closing, the *mushroom* was placed at 20 ± 2 °C for 1 week, and then the precipitated particles were isolated by several cycles of centrifugation with deionized water, freeze-dried at −60 °C under vacuum (3 mbar) overnight, and stored until further characterizations. The experiments were performed in triplicate. A few seconds after mixing the reagents and just before closing the *mushroom*, a white viscous suspension started to be formed. To analyze this first precipitate, we took a sample of this suspension and immediately washed it with ultrapure water and then with ethanol and dried it by ethanol evaporation.

Characterization Techniques. The pH of the droplets was measured using a pH electrode (Titan model, Sentron) placed in a hole located on a sidewall of the crystallization chamber (Figure 2). The evolution of the precipitation in the droplets was repeatedly observed *in situ* using an optical microscope (Leica MZ12 or Olympus SZH10) connected to a digital camera (Olympus, C3040ZOOM). The morphology of the precipitates was characterized by transmission electron microscopy (TEM). In addition, the nature and the composition of some particles observed with TEM were simultaneously analyzed by selected area electron diffraction (SAED) and energy-dispersive X-ray spectroscopy (EDS). These experiments were carried out with a Philips CM 100 instrument operated at 80 kV. The powdered samples were ultrasonically dispersed in ultrapure water, and then a few droplets of the slurry were deposited on Formvar/carbon copper grids. Additionally, the structural and physicochemical properties of the precipitates were analyzed by powder X-ray diffraction (PXRD) and Fourier transform infrared spectroscopy (FTIR). PXRD patterns were collected with a Panalytical X'Pert Pro powder diffractometer equipped with an X'Celerator detector, using Cu Kα radiation generated at 40 kV and 40 mA. The instrument was configured with 1/2° both divergence and receiving slits. The 2θ range was from 10° to 60°, with a step size of 0.02° and a time per step of 104 s. The sample was ground and placed on a quartz sample holder. However, the crystalline precipitates obtained in the presence of 30 and 60 mM L-Asp were not enough to be analyzed by PXRD. Therefore, the crystals were ground and mounted on a Bruker X8 Proteum diffractometer equipped with a Microstar copper rotating anode generator, a κ goniometer, and a SMART 6000 CCD detector. The calculated powder pattern was obtained after integrating the diffraction frames with the XRD2DSCAN software.[25] FTIR spectra were recorded on a Thermo Nicolet 380 FT-IR spectrometer. Each powdered sample (~1 mg) was mixed with about 100 mg of anhydrous KBr and pressed into 7 mm diameter discs. Pure KBr discs were used as background. The infrared spectra were collected from 4000 cm^{-1} to 400 cm^{-1} with a resolution of 2 cm^{-1}.

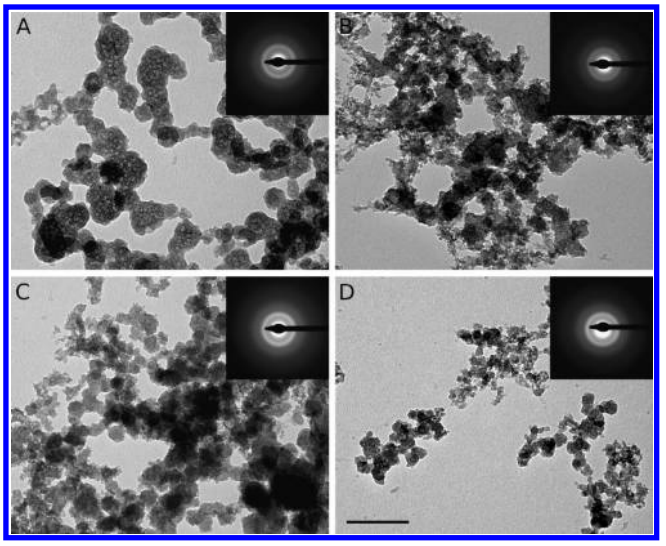

Figure 3. TEM images of ACP precipitated a few seconds after mixing the solutions: (A) in the absence of amino acids or (B) in the presence of 30 mM L-aspartic acid; (C) 30 mM L-alanine; (D) 30 mM L-arginine. Scale bar = 200 nm.

RESULTS

Early Stages in Calcium Phosphate Precipitation. TEM analysis of the dried precipitates obtained a few seconds after mixing the solutions revealed that the early precipitated phase was composed of chains of spherules (Figure 3) whose chemical composition, analyzed by EDS, consisted of Ca, O, and P. In addition, they did not show any distinguishable SAED pattern but diffuse rings (insets of Figure 3), indicating that these

Table 1. Effects of Acidic and Basic Amino Acids on the Crystallization of CaP with the VDSD Method[a]

amino acid conc	TEM-SAED information	PXRD and FTIR	initial and final pH
blank	**HA (50−120 nm)**, (OCP)	**HA**	5.4−8.2
L-Asp 5 mM	**HA**, flower-like HA, (DCPD)	**HA**	5.7−8.4
L-Asp 30 mM	**DCPD**, (HA)	**DCPD**	4.5−6.9
L-Asp 60 mM	**DCPD**, (HA)	**DCPD**	4.2−5.8
L-Asp 60 mM (HEPES buffer)		**HA**, (OCP)	8.5−7.5
L-Ala 5 mM	**OCP**, (HA)	**OCP, HA**	5.8−9.0
L-Ala 30 mM	**flower-like HA, OCP**	**OCP, HA**	5.9−8.2
L-Ala 60 mM	**OCP, HA (200−300 nm)**	**OCP, HA**	6.3−7.6
L-Arg 5 mM	**OCP**, (HA), (OCP)	**OCP**, (HA)	7.1−8.5
L-Arg 30 mM	**HA (20−40 nm)**, (OCP)	**HA**	8.8−9.1
L-Arg 60 mM	**HA (20−40 nm)**, (OCP),	**HA**	9.1−8.3

[a] Main phases are in bold characters. Minority phases are indicated in parentheses.

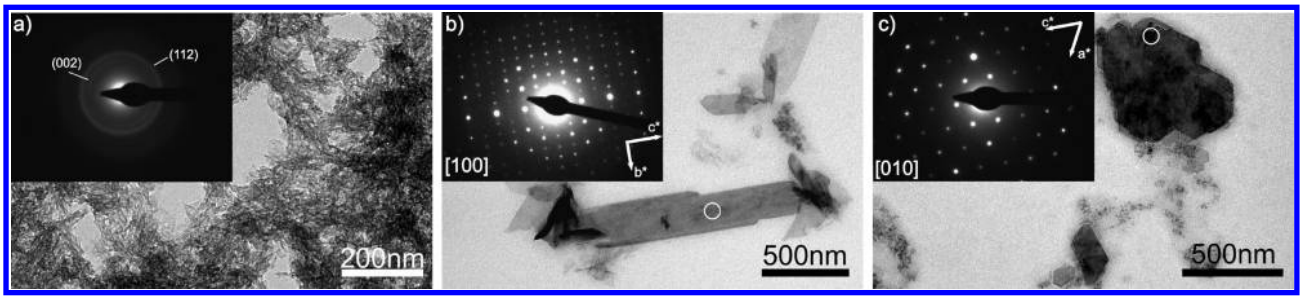

Figure 4. TEM micrographs and corresponding SAEDs of the different calcium phosphates: (a) HA nanoparticles (ASTM card file no. 9-432); (b) OCP (ASTM card file no. 26-1056); (c) DCPD (ASTM card file no. 9-77). Vectors of the reciprocal lattice for OCP and DCPD single crystals are also indicated. The SAED patterns in parts b and c were obtained from the areas marked with white circles.

particles were amorphous calcium phosphate (ACP).[26] The occurrence of an initial ACP phase was independent of the nature and concentration of the amino acid added to the solution.

Amino Acidic Effect on Calcium Phosphate Precipitation. The pH evolutions strongly depend on the type of amino acid added to the solution during the crystallization of CaP with the VDSD micromethod (see Table 1). In the absence of amino acids (blank experiment), the pH value increased gradually from 5.4 to reach a plateau of pH 8.2 in 7 days. In the presence of 30 mM L-asp and 30 mM L-ala, it rose from 4.5 to 6.9 and from 5.9 to 8.2, respectively. In the presence of 30 mM L-arg, the pH rapidly decreased to 5.9 and subsequently gradually rose to 9.1. The latter behavior was also observed when using 5 mM and 60 mM L-arginine.

Depending on the nature and the concentration of the amino acid added, 7 days after vapor diffusion, different CaP phases were observed (see Table 1 hereafter). In particular from SAED patterns (Figure 4), the following CaP phases were identified: (i) HA particles (misoriented) characterized by rings at the *d*-spacings 3.44 and 2.78 Å, corresponding to the (002) and (112) HA crystallographic planes, respectively; (ii) OCP; and (iii) DCPD. Micrometric-sized OCP (Figure 4b) and DCPD (Figure 4c) single crystals showed preferential orientation along the *c*-axis.

In the blank experiment, we mainly observed platelike HA nanoparticles whose dimensions ranged between 50 and 130 nm (Figure 5a). Figure 6.1.b shows the PXRD pattern of this sample. It displays the characteristic HA diffraction peak at 25.90° related with the (002) plane, as well as a broad peak due to the triplet [(211), (112), and (300)] (ASTM card file no. 9-432), suggesting that HA is the main phase forming the precipitated particles. The presence of broad reflections in the diffraction pattern is indicative of the precipitation of poorly crystalline HA nanoparticles. In addition, no peaks related to the OCP phase are detectable. Concerning the spectroscopic information of this sample, the FTIR spectrum (Figure 6.2.b) fitted remarkably well with the FTIR spectrum previously reported for the pure HA phase.[27,28] It displayed a main broad band at 1032 cm^{-1} with shoulders at ca. 1046 and 1075 cm^{-1} assignable to the triply degenerated asymmetric stretching mode of the PO_4 groups (ν_3PO_4). At *ca.* 961 cm^{-1} a shoulder appeaed due to the nondegenerated symmetric stretching mode (ν_1) of the PO_4 groups.[27,28] Moreover, features at *ca.* 601, 576 (shoulder), and 560 cm^{-1} related with the triply degenerated bending mode (ν_4) of the PO_4 groups could also be recognized.[27,28] Also in this case, none of the bands assignable to the presence of the OCP phase was detected, confirming that carbonate-HA was the main phase. In addition, both A- and B-type substitutions (carbonate replacing hydroxyl and phosphate positions in the HA crystal lattice, respectively) took place, as suggested by the bands at *ca.* 1556 and 880 cm^{-1} and 1450, 1420, and 873 cm^{-1}, respectively.[27,29] The intensity of these bands clearly indicates that B-type substitutions, instead of A-type substitutions, were strongly favored.

When L-asp (iep = 2.77) was added to the drops up to the final concentrations of 5 mM, in most precipitates HA in two different morphologies was found, i.e. needle-like particles of around 150−200 nm forming larger spherical aggregates and flower-like particles composed of lamellae (not shown). When increasing the concentration of L-asp up to 30 mM, besides a low amount of needles HA, platelets with irregular shapes but with edges of

varying dimensions, typically from 200 nm to 100 μm approximately, were observed. Even in some zones of the drops, platelets up to 700 μm in length were found. SAED patterns (Figure 4c) identified these platelets as DCPD (brushite). The XRD pattern (Figure 6.1.a) and FTIR spectrum (Figure 6.2.a) of these crystals also confirmed that they were DCPD. However, the presence of weak shoulders in the FTIR spectrum at *ca.* 1034 and 1075 cm^{-1} could also indicate the presence of a small percentage of HA particles precipitated together with the main DCPD phase, as observed also in TEM micrographs. The results obtained with the highest concentration (60 mM) of L-asp were identical. Finally, the PXRD and FTIR characterization of the precipitate using 60 mM L-asp and HEPES buffer indicate the presence of HA with OCP as a minor component (not shown).

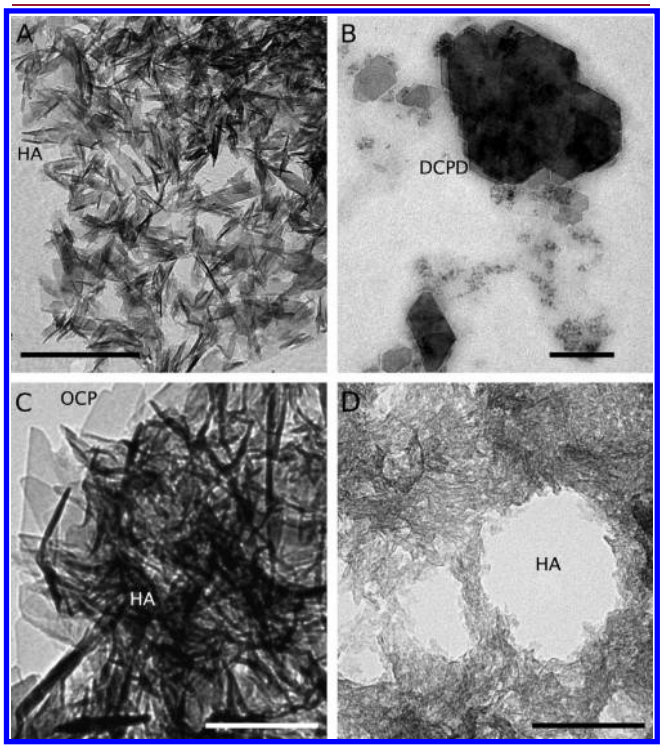

Figure 5. TEM images of the different CaP phases precipitated after 7 days of vapor diffusion: (A) HA nanoparticles in the blank experiment; (B) DCPD in the presence of 30 mM L-asp; (C) OCP and HA in the presence of 30 mM L-ala; (D) HA nanoparticles in the presence of 30 mM L-arg. Scale bar = 200 nm.

In the presence of 5 mM L-ala, the precipitates were mostly composed of elongated platelets of different length reaching about 1 μm. The SAED patterns of these crystals correspond to OCP (Figure 4b). When increasing the concentration of L-ala up to 30 mM, OCP platelets and needle-like HA with typical length between 150 and 200 nm were mainly found (Figure 5c). PXRD patterns confirm the presence of both phases (Figure 6.1.c). In this case, other peaks appeared at the 2θ angles 9.45°, 9.77°, 16.05°, and 24.30° (marked with circles), due to the presence of OCP in the precipitate (ASTM card file no. 26-1056). Moreover, the FTIR spectrum (Figure 6.2.c) displayed the typical bands of the HA phase together with bands at ca. 1123, 1105, 916, and 526 cm^{-1} related to the $\nu_1HPO_4^{2}$, $\nu_3HPO_4^{2-}$, and $\nu_4HPO_4^{2-}$ vibrational modes of the OCP phase.[27,30] The unusually high intensity and the shift to higher 2θ angles of the (002) peak are due to the preferential orientation of the OCP crystals along the *c*-axis, as previously observed in TEM micrographs (Figure 4b). The full width at half-maximum (fwhm) of the ν_4 PO_4 mode band appearing at ca. 601 cm^{-1} decreased compared with that obtained in the absence of amino acid (Figure 6.2.b), indicating the formation of larger crystalline domains in the presence of this amino acid.[28,31] Additionally, as discussed above, the pH was lower in the presence of this amino acid, and this finding could explain the low intensity of the carbonate bands. When the concentration of L-ala increased to 60 mM, OCP platelets up to 60−70 μm in length were obtained, although the main phase was HA.

Finally, the situation changed when adding L-arg to the reaction mixture. At 5 mM L-arg, TEM observations indicate that OCP was the major phase while HA was the minor one.

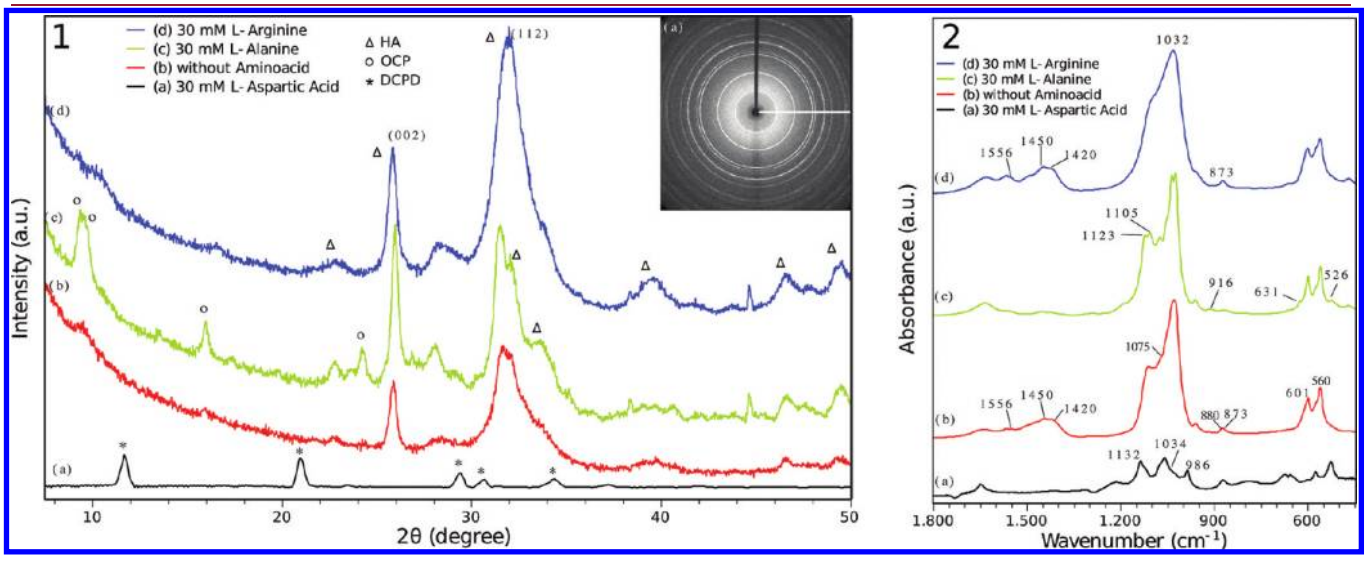

Figure 6. (1) X-ray powder diffraction patterns of precipitates obtained in the absence of amino acids (b) or in the presence of 30 mM L-ala (c), 30 mM L-arg (d), or 30 mM L-asp (a). The latter was obtained after integrating along the marked line of the single crystal diffraction pattern (inset) using the XRD2DSCAN software.[2525] (2) FTIR spectra of the precipitates obtained in the absence of amino acids (b) and in the presence of 30 mM of L-asp (a), 30 mM L-ala (c), or 30 mM L-arg (d).

dx.doi.org/10.1021/cg2004547 |*Cryst. Growth Des.* 2011, 11, 4802–4809

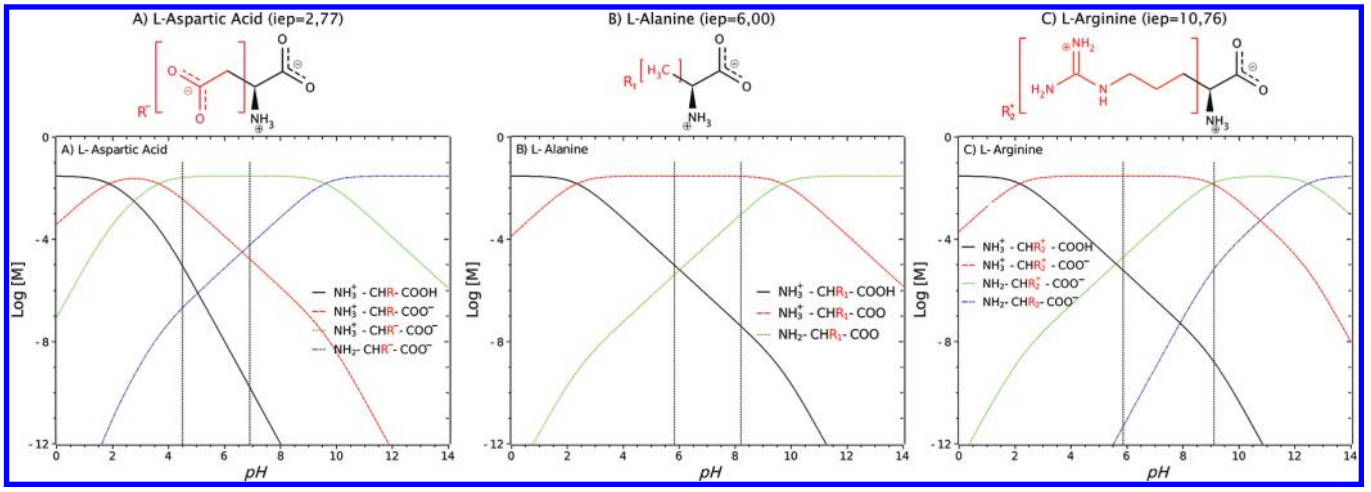

Figure 7. Evolution of amino acidic ionic species as a function of the pH: (A) 30 mM L-aspartic acid, (B) 30 mM L-alanine, and (C) 30 mM L-arginine. The dotted vertical lines in the graphs represent the pH range in the vapor diffusion experiments.

However, at 30 and 60 mM L-arg, TEM images clearly showed HA nanoparticles of 20−40 nm in length as the major phase (Figure 5d). Only a few small OCP crystals were detected. The result was confirmed by PXRD and FTIR data (Figure 6.1.d and 6.2.d, respectively). The PXRD pattern was similar to that reported for typical poorly crystalline HA.[32,33] The FTIR spectrum was the same as that obtained in the absence of amino acid (Figure 6.2.b) but with broader bands indicating lower crystallinity and shorter crystalline domains size[28] of the HA grown in the presence of L-arg. The typical carbonate IR absorption bands suggest that, as in the absence of amino acids, both A- and B- type substitutions were present in the carbonate-HA nanoparticles, with B-type substitutions being strongly favored. The amount of substituted carbonate (known as carbonation degree[31]) can be estimated as the area ratio of the ν_2CO_3 (894−862 cm^{-1}) over the ν_3PO_4 (1184−910 cm^{-1}) regions. The carbonation degree estimated for the particles grown in the presence of 30 mM of L-arg was around 3.5%, being rather higher in the absence of amino acid (3.8%). These values closely resemble the amount of carbonate in the bone nanoapatite crystals.[1,5]

DISCUSSION

The results of the present work demonstrate that selected amino acids at given concentrations, when using the VDSD technique, can be used as polymorph directing agents in CaP precipitation. Additionally, it has been shown that, by using L-arg in 30−60 mM concentrations, it is possible to obtain nanocrystalline HA with properties similar to those of bone HA: i.e. length between 20 and 40 nm and 3.5% w/w carbonate content mainly in B-positions.[1,6] So far, there has not been clear evidence in the FTIR spectra about the incorporation and/or adsorption of amino acids or other molecules, e.g. acetate, on CaP precipitates in spite of the clear effects of amino acids on polymorph selection and size distribution. Indeed, adsorbed amino acids were only reported to be detected on nanocrystalline HA prepared by a semibatch precipitation macromethod when a 150 mM amino acid concentration and constant pH = 10[13] were used. Probably, in our case, the amount of adsorbed amino acids was not enough to be detected by FTIR. In addition, the main bands of L-ala and L-arg, related to amino and carboxylate groups, should appear in the range from 1400 to 1650 cm^{-1}, which is the typical region of carbonate-substitutions and physisorbed water molecule bands,[34] so it is difficult to determine with certainty the presence of adsorbed amino acids.

When employing the VDSD micromethod with L-asp, L-ala, and L-arg, the first transient phase formed at any amino acid concentration tested was ACP. However, the effects of the amino acids on the pathway to obtain the most stable phase HA with given morphologic and chemical features varied according to the nature of the amino acid. Indeed, in the presence of higher concentrations of L-asp, the precipitation of DCPD was favored against that of HA (see Table 1). This was attributed both to the simultaneous action of the amino acid on the pH evolution of the droplets (from 4.5 to 6.9 at 30 mM versus 5.4 to 8.2 in the blank experiment) and to the strong electrostatic interaction that occurs at these pH values between the deprotonated carboxylic acids of major $NH_3^+-CHR^-COO^-$ forms of the L-asp (Figure 7a) and the $>Ca^{\delta+}$ sites on the brushite surface, thus slowing down or inhibiting its further transformation to HA. The specific adsorption of this amino acid on the (010) face of DCPD explains the preferential orientation of this crystal along the *c*-axis (Figure 4c). However, when using 60 mM L-asp together with HEPES buffer, the pH evolution is different (8.5−5.5−7.5), and as a consequence, the composition of the precipitate was mainly HA with a small amount of OCP. In the presence of 30 mM L-ala, the pH of the experiment increased from 5.9 to 8.2 and the pathway to obtain HA was via OCP. In this pH range, OCP together with HA were the major precipitated solid phases. As commented above, the unusual high intensity of the (002) reflection of OCP in the XPRD pattern (Figure 6.1.c) is most probably due to orientation of the OCP crystals along the *c*-axis. At these pH values the zwitterionic forms of L-ala ($NH_3^+-CHR_1-COO^-$) were the dominant species (Figure 7b). They could interact electrostatically either through their deprotonated carboxylate with the $>Ca^{\delta+}$ sites or through their $-NH_3^+$ groups with the $>PO_4^{\delta-}$ sites of the OCP surface. Also, weak H-bonding could be formed between the $-NH_3^+$ and neutral phosphate surface groups, such as $>PO_4H_2$. The bifunctional nature of this zwitterionic form was responsible for the weak inhibition of the OCP to HA transformation and the reason by which a mixture of the two polymorphs was obtained in a pH range that was almost similar to that found in the control experiment. The specific adsorption of this amino acid on the (001) face of

dx.doi.org/10.1021/cg2004547 |*Cryst. Growth Des.* 2011, 11, 4802–4809

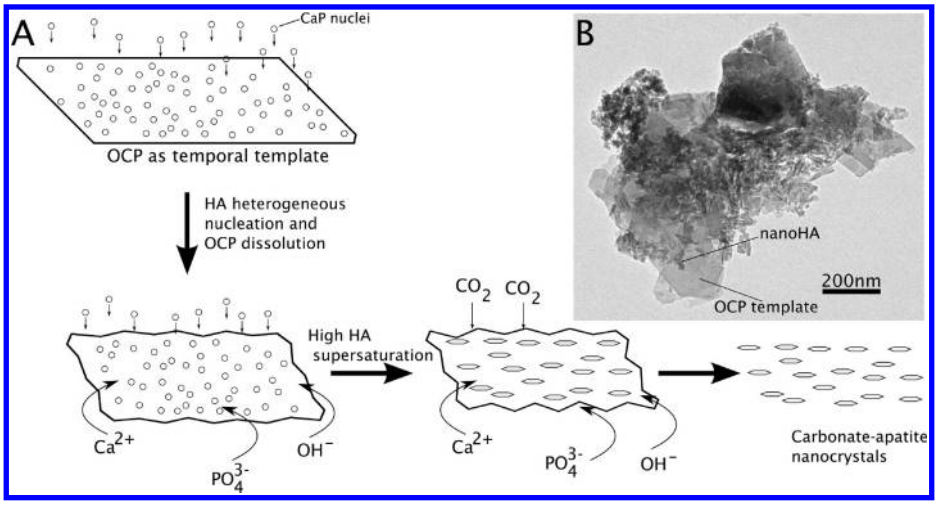

Figure 8. (A) Schematic model of the formation of carbonate-HA nanoparticles on OCP substrates acting as temporal templates. (B) TEM micrograph of HA nanoparticles grown on OCP platelets.

OCP explains its preferential orientation. An oriented attachment mechanism for OCP formation, well-known in the vapor diffusion technique[35] for other crystals such as $CaCO_3$ (vaterite), could be a likely mechanism of crystal formation.

When using 30 mM L-arg (pH goes from 8.8 to 5.8 and then rises to 9.1), the main ionic species were $NH_3^+-CHR_2^+-COO^-$ and $NH_2-CHR^+-COO^-$ (Figure 7c) and the most likely interaction of the amino acid with the OCP surface was weak H-bonds by means of their $-NH_3^+$ residues. Under these chemical conditions, the OCP to HA transformation was weakly inhibited and the pathway to obtain HA was very similar to that of the control. In the precipitates obtained in both experiments (control and L-arg added), there was a scarce presence of OCP because of the high extent of the OCP to HA transformation.

Model of Formation of HA Nanoparticles. It is commonly accepted that OCP is a precursor of the HA formation.[33,36] Under neutral or basic conditions the metastable phase OCP transforms to HA through dissolution and recrystallization processes, following the Ostwald rule of stages.[37] Also, it was demonstrated that the formation of HA on OCP is an epitaxial process.[38] What is still unsolved is the mechanism by which HA is obtained in nanometric or micrometric size. An interesting observation in the present work was the presence of nanocrystals closely linked to the OCP surface (Figure 8B) in the blank experiment and when using 30 and 60 mM L-arg. This finding suggests that OCP could act as a temporal template for the formation of nanosized HA. The hypothesis is based on the similarity with previous findings of nanosized HA in the system Ca-citrate/phosphate/H_2O[24] and of nanocalcite in the system $Ca(OH)_2-CO_2-H_2O$,[39] where a temporal template was responsible for the formation of the HA and calcite with nanometric sizes. The role of the template mainly consists on the stabilization of the newly heterogeneously nucleated crystals with nanometric sizes. Indeed, the precipitation of HA at high supersaturation values (obtained at the highest pH values of these experiments) leads to the formation of a high amount of supercritical nuclei (defined here as the clusters having a radius higher than that of the critical nucleus). The decrease of Gibbs free energy in that system can be produced not only by growth of these supercritical nuclei but also by primary aggregation of the growing particles with nanometer size. The template might interact with the primary particles formed by heterogeneous nucleation, stabilizing them and, thus, minimizing their aggregation tendency. The result is the production of nanosized crystals, at the same time that the template dissolves (Figure 8A).

The precipitation of a temporal substrate for the formation of nanosized HA was previously demonstrated during the precipitation of this material from a Ca/citrate/phosphate solution using microwave and conventional heating.[24] In this system, the precipitation of a sodium citrate precipitate of composition $Na_3(cit)\cdot 2H_2O$ during the first minutes of the experiment acted as a temporal template for the formation of HA with nanometric size. In the absence of this template, crystals grew until submicrometric or micrometric sizes.

CONCLUSIONS

This paper highlights the important role that amino acids have as regulators of the CaP precipitation process, influencing both the solution pH (depending on their isoelectric points) and/or the transformation of the precursor phase (which will depend on the nature and strength of the interaction taking place at the amino acid/inorganic interface). In addition, it provides a thermodynamic formation model of nanocrystalline HA mediated by a temporal OCP template. The model is based on the analogy of the formation of nanosized HA in this system with that of nanosized HA in the Ca-citrate/phosphate/H_2O[24] and of nanocalcite in the $Ca(OH)_2-CO_2-H_2O$[37] systems, and it is supported by TEM observations.

Acidic and basic amino acids influence differently the precipitation mechanism of CaP when using the VDSD micromethod. The early stage in the precipitation, irrespective of the nature and the concentration of the amino acid used, leads to the formation of a viscous suspension composed of ACP spherulites. Nevertheless, with higher concentrations of L-asp, the precipitation of DCPD takes place, whereas, in the presence of higher concentrations of L-ala, both HA and OCP precipitate. Only when L-arg is added to the droplets is the precipitation of the HA phase favored relative to OCP, as observed in the control experiment. This finding is related to the influence of these amino acids on the pH of the solutions and the strength of the interaction of major charged species of these amino acids with the

surface calcium and phosphate groups in the precursor phase DCPD or OCP. Moreover, in the presence of 30 and 60 mM L-arg, the precipitates are composed of carbonated-HA nanocrystals within the 20−40 nm size range, which is similar to that of bone HA nanocrystals. The precipitation of carbonate-HA nanocrystals in the control experiment and in the presence of L-arg is most probably explained by the combination of (a) a higher pH and therefore a higher supersaturation of mother solutions relative to HA, and (b) the presence of OCP, which is the metastable precursor phase and, at the same time, acts as a temporal template which stabilizes the primary supercritical nuclei in a nanometric size, avoiding their tendency to enlarge either by growth or by aggregation.

AUTHOR INFORMATION

Corresponding Author

*E-mail: jaime@lec.csic.es. Telephone: +34 958 230000. Fax: +34 958 552620.

ACKNOWLEDGMENT

The authors greatly acknowledge the Spanish Ministerio de Ciencia e Innovación (MICINN) for support (Spanish−Italian Integrated Action refs. IT2009-00028 and MAT2011-28543). J.G.-M., J.M.D.-L., and A.H.-H. belong to the research team *"Factoría de Crystalización" (Consolider Ingenio 2010)* of the Spanish MICINN. J.M.D.-L. also thanks the Consejo Superior de Investigaciones Científicas (CSIC) for his postdoctoral JAE-DOC research contract. M.I. is the recipient of a fellowship from Regione Piemonte and acknowledges the Research project "Nanoparticelle multifunzionali per la terapia dei carcinomi: studi in vitro e in vivo in modelli sperimentali", being funded by Regione Piemonte (Ricerca Sanitaria Finalizzata 2009, Grant no. 30258/DB2001) and the InterUniversity Consortium for Research on Chemistry of Metals in Biological Systems (C.I.R.C.M.S.B).

REFERENCES

(1) Lowenstam, H. A.; Weiner, S. *On Biomineralization*; University Press: Oxford, 1989.
(2) Currey, J. D. *Osteoporosis Int.* **2003**, *14*, 29–36.
(3) Estroff, L. A.; Hamilton, A. D. *Chem. Mater.* **2001**, *13*, 3227–3235.
(4) Glimcher, M. J. In *Metabolic Bone Disease and Clinically Related Disorders*, 3 ed.; Avioli, L. V., Krane, S. M., Eds; Academic Press: San Diego, CA, 1998; pp 23−50.
(5) Dorozhkin, S. V.; Epple, M. *Angew. Chem., Int. Ed.* **2002**, *41*, 3130–3146.
(6) Eichert, C.; Drouet, C.; Sfihi, H.; Rey, C.; Combes, C. In *Biomaterials Research Advances*; Kendall, J. B., Ed.; Nova Science Publishers: 2007; pp 93−143.
(7) Wang, L.; Nancollas, G. H. *Chem. Rev.* **2008**, *108*, 4628–4669.
(8) Hafiz Uddin, M.; Matsumoto, T.; Ishihara, S.; Nakahira, A.; Okazaki, M.; Sohmura, T. *J. Dent. Res.* **2010**, *89*, 488–492.
(9) Koutsopoulos, S.; Dalas, E. *J. Cryst. Growth* **2000**, *217*, 410–415.
(10) Matsumoto, T.; Okazaki, M.; Inoue, M.; Sasaki, J. I.; Hamada, Y.; Takahashi, J. *Dent. Mater. J.* **2006**, *25*, 360–364.
(11) Ikawa, N.; Kimura, T.; Oumi, Y.; Sano, T. *J. Mater. Chem.* **2009**, *19*, 4906–4913.
(12) Pan, H. H.; Tao, J. H.; Xu, X. R.; Tang, R. K. *Langmuir* **2007**, *23*, 8972–8981.
(13) Palazzo, B.; Walsh, D.; Iafisco, M.; Foresti, E.; Bertinetti, L.; Martra, G.; Bianchi, C. L.; Cappelletti, G.; Roveri, N. *Acta Biomater.* **2009**, *5*, 1241–1252.
(14) Dorozhkin, S. V. *Acta Biomater.* **2010**, *6*, 715–734.
(15) Iafisco, M.; Gómez-Morales, J.; Hernández-Hernández, M. A.; García-Ruiz, J. M.; Roveri, N. *Adv. Eng. Mater.* **2010**, *12*, B218–B223.
(16) Iafisco, M.; Delgado-López, J. M.; Gómez-Morales, J.; Hernández-Hernández, M. A.; Rodríguez-Ruiz, I.; Roveri, N. *Cryst. Res. Technol.* **2011**, *46*, 841–846.
(17) Gómez-Morales, J.; Hernández-Hernandez, A.; Sazaki, G.; García-Ruiz, J. M. *Cryst. Growth Des.* **2010**, *10*, 963–969.
(18) Hernández-Hernandez, A.; Rodríguez-Navarro, A. B.; Gómez-Morales, J.; Jimenez-Lopez, C.; Nys, Y.; Garcia-Ruiz, J. M. *Cryst. Growth Des.* **2008**, *8*, 1495–1502.
(19) Hernández-Hernández, A.; Gómez-Morales, J.; Rodríguez-Navarro, A. B.; Gautron, J.; Nys, Y.; García-Ruiz, J. M. *Cryst. Growth Des.* **2008**, *8*, 4330–4339.
(20) Nassif, N.; Gobeaux, F.; Seto, J.; Belamie, E.; Davidson, P.; Panine, P.; Mosser, G.; Fratzl, P.; Giraud Guille, M.-M. *Chem. Mater.* **2010**, *22*, 3307–3309.
(21) Nassif, N.; Martineau, F.; Syzgantseva, O.; Gobeaux, F.; Willinger, M.; Coradin, T.; Cassaignon, S.; Azais, T.; Giraud-Guille, M. M. *Chem. Mater.* **2010**, *22*, 3653–3663.
(22) *CRC Handbook of Chemistry and Physics*, 71th ed.; CRC Press: Boca Ratón, FL, 1990.
(23) Gustafsson, J. P. *Visual MINTEQ 3.0, Computer Program for Calculating Aqueous Geochemical Equilibria*; 2011; adapted from MINTEQA2 (CEAM, EPA, 1999).
(24) López-Macipe, A.; Gómez-Morales, J.; Rodríguez-Clemente, R. *Adv. Mater.* **1998**, *10*, 49.
(25) Rodriguez-Navarro, A. B. *J. Appl. Crystallogr.* **2006**, *39*, 905–909.
(26) Yang, X.; Xie, B.; Wang, L.; Qin, Y.; Henneman, Z. J.; Nancollas, G. H. *CrystEngComm* **2011**, *13*, 1153–1158.
(27) Koutsopoulos, S. *J. Biomed. Mater. Res.* **2002**, *62*, 600–612.
(28) Antonakos, A.; Liarokapis, E.; Leventouri, T. *Biomaterials* **2007**, *28*, 3043–3054.
(29) Xu, G.; Aksay, I. A.; Groves, J. T. *J. Am. Chem. Soc.* **2001**, *123*, 2196–2203.
(30) Fowler, B. O.; Markovic, M.; Brown, W. E. *Chem. Mater.* **1993**, *5*, 1417–1423.
(31) Bala, Y.; Farlay, D.; Delmas, P. D.; Meunier, P. J.; Boivin, G. *Bone* **2010**, *46*, 1204–1212.
(32) Liao, S.; Watari, F.; Xu, G.; Ngiam, M.; Ramakrishna, S.; Chan, C. K. *Mater. Lett.* **2007**, *61*, 3624–3628.
(33) Rey, C.; Combes, C.; Drouet, C.; Glimcher, M. J. *Osteoporosis Int.* **2009**, *20*, 1013–1021.
(34) Socrates, G. *Infrared and Raman Characteristic Group Frequencies*; John Wiley & Sons: Chichester, 2001.
(35) Gehrke, N.; Cölfen, H.; Pinna, N.; Antonietti, M.; Nassif, N. *Cryst. Growth Des.* **2005**, *5*, 1317–1319.
(36) Lu, X.; Leng, Y. *Biomaterials* **2005**, *26*, 1097–1108.
(37) Zhan, J. H.; Tseng, Y. H.; Chan, J. C. C.; Mou, C. Y. *Adv. Funct. Mater.* **2005**, *15*, 2005–2010.
(38) Tseng, Y.-H.; Mou, C.-Y.; Chan, J. C. C. *J. Am. Chem. Soc.* **2006**, *128*, 6909–6918.
(39) García-Carmona, J.; Gómez-Morales, J.; Rodríguez-Clemente, R. *J. Cryst. Growth* **2003**, *249*, 561–571.